CrystEngComm

Accepted Manuscript

ROYAL SOCIETY OF CHEMISTRY

www.rsc.org/crystengcomm

Cite this: DOI: 10.1039/c0xx00000x

www.rsc.org/xxxxxx

ARTICLE TYPE

Metal Ion-Mediated Synthesis and Shape-dependent Magnetic Properties of Single-Crystalline α-Fe_2O_3 Nanoparticles

Wei Wu *[a, b, #], Shuanglei Yang[c, #], Jun Pan[c], Lingling Sun[b], Juan Zhou[b], Zhigao Dai[b], Xiangheng Xiao[b], Hongbo Zhang[c], Changzhong Jiang[b]*

Received (in XXX, XXX) Xth XXXXXXXXX 20XX, Accepted Xth XXXXXXXXX 20XX
DOI: 10.1039/b000000x

A facile and effective hydrothermal process for the controllable synthesis of uniform single-crystalline hematite (α-Fe_2O_3) nanoparticles with different shapes is presented. The morphology of the α-Fe_2O_3 products can be controlled through simply adjusting the metal ions additive. The effects of the different metal ions (atomic number from 25-30) on the size and morphology of the products were investigated. The cubic and thorhombic α-Fe_2O_3 particles can be generated by adding the zinc ions and copper ions in the reaction process, respectively. For providing some insight into the correlation between the morphology and physicochemical properties, the magnetic properties of the as-obtained cubic and thorhombic α-Fe_2O_3 products were investigated. Interesting, the cubic α-Fe_2O_3 products exhibited a superparamagnetic properties at T = 300 K. In contrast, the thorhombic α-Fe_2O_3 products displayed ferromagnetic and low-temperature phase transition behaviours at room temperature. The fundamental understanding of crystal-phase and morphology-tunable nanostructures that are enclosed by shape-dependent magnetic properties is expected to direct the design and development of highly efficient magnetic nanomaterials.

1. Introduction

In recent years, great efforts have already been devoted to the development of nanomaterials with well-defined and controllable morphologies. It is well known that controlling the size, phase, shape and dimensionality of inorganic nano/microstructures is fundamental and technological importance because of the strong correlation between these parameters and their chemical/physical characteristics, such as magnetic, optical and catalytic properties, as well as distinctly affect their potential applications in many fields.[1-5] Moreover, the search for new geometries is an important aspect for magnetic iron oxide nanomaterials, and previous researches mainly focus on low-demension nanoparticles.[1, 6] Generally, the lowest energy state of a magnetic particle depends on its size, shape, strength and character of its anisotropy, especially the shape of nanomaterials can influence its magnetic properties in different ways.[7] Magnetic quantities such as anisotropy and coercivity are important for many present and future applications in permanent magnetism, magnetic recording, and spin electronics.[8]

Magnetic iron oxide nanoparticles play important roles in many different areas, and hence understanding the correlation between the magnetic properties and the morphology of nanostructures is a prerequisite for widespread applications. Moreover, skilful synthesis of magnetic nanoparticles with tunable morphology will be the top priority since the ultimate goal of morphology dependent magnetic iron oxide-based catalyst is to design and fabricate catalytic materials that can expose more active sites within a uniform nanostructure.[9-13] As the most stable iron oxide and n-type semiconductor properties under ambient conditions, hematite (α-Fe_2O_3) is widely used in pigments, catalysts, and gas sensors owing to its low cost and high resistance to corrosion, and it can be used as the starting material for the synthesis of magnetite (Fe_3O_4) and maghemite (γ-Fe_2O_3), which have been intensively pursued for both fundamental scientific interest and technological applications in the last few decades. In order to highlight some special properties demanded by particular technological applications, various hematite nanostructures have been synthesized, such as nanoparticles, nanowires, nanorings, nanotubes, etc.[14-17] Recently, cation or anion exchange on the nanoscale have become an emerging technique for new material synthesis, device fabrication, and chemical sensing.[18] For α-Fe_2O_3, the surface energies of the low-index planes are close to each other; accordingly, the stability order of these planes may be changed quite easily through the preferential adsorption of ionic species or small alterations in the reaction conditions.[19-22] For example, Lv and co-workers have reported highly symmetric dodecahedral and octodecahedral single crystalline α-Fe_2O_3 particles have been successfully synthesized with the aid of F^- anions using a facile hydrothermal method. The dodecahedral and octodecahedral α-Fe_2O_3 particles possessed coercivities of 4986 Oe and 6512 Oe, respectively, showing much stronger magnetism than the

Cite this: DOI: 10.1039/c0xx00000x

www.rsc.org/xxxxxx

ARTICLE TYPE

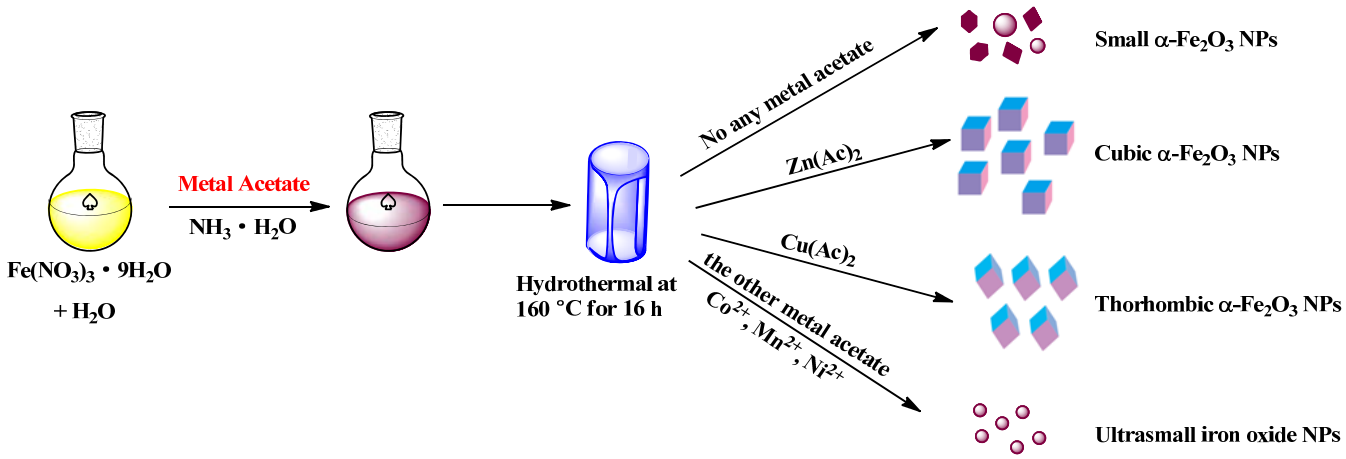

Scheme 1 Schematic illustration of the synthesis of hematite in various shape depending on the different metal ions.

previously reported α-Fe_2O_3 nanoparticles.[23] More recently, Choi and co-workers have reported that different shapes of Fe_3O_4 nanoparticles, including solid nanospheres and solid and hollow nanoellipsoids, could be obtained by either adding the appropriate amount of sodium acetate (NaOAc) or using the anion exchange of the precursor of β-FeOOH. It is also proposed that chloride ions in the β-FeOOH structure play a key role in the formation of a hollow structure.[24]

Herein, we demonstrate a template-free wet-chemical process to prepare single-crystalline hematite particles with different shapes, which depends on the additive of metal ions in the reaction (as shown in **Scheme 1**). The fabricated α-Fe_2O_3 particles present regular cubic or thorhombic shapes with six facets. More interestingly, the edge length of cubic and thorhombic particles is almost equally. Moreover, their magnetic properties depending on shape and crystalline structure were investigated in detail. The cubic α-Fe_2O_3 particles exhibit the superparamagnetic behaviours at T = 300 K. However, the thorhombic α-Fe_2O_3 particles exhibit the ferromagnetic behaviours. We expect that it is possible to understand more accurately the shape-dependent magnetic properties through our method.

2. Experimental Section

2.1 ***Materials.*** Iron (III) nitrate nonahydrate ($Fe(NO_3)_3·9H_2O$, AR), zinc acetate ($Zn(CH_3COO)_2·2H_2O$, AR), cupric acetate anhydrous ($Cu(CH_3COO)_2$, AR) and ammonia solution (25%, AR) were purchased from Sinopharm Chemical Reagent CO., Ltd., and all used as received without further purification. The MagneticSphere Technology Magnetic Separation Stand (MSS), purchased from Promega (Z5333), was used to separate magnetic particles at washing and selecting steps.

2.2 ***Synthesis of cubic and thorhombic α-Fe_2O_3 particles.*** The hematite particles were prepared by a hydrothermal treatment of iron (III) nitrate with zinc and cupric ions additives. In a typical experimental procedure, 0.808 g $Fe(NO_3)_3·9H_2O$ was dissolved in 10 mL water under magnetic stirring, and then 0.1 mol acetate precursor was added in the above solution, after 10 min, 10 mL ammonia solution was added. After 10 min of stirring, the mixture was transferred into a Teflon-lined stainless steel autoclave with a capacity of 50 mL for hydrothermal treatment. The autoclave was sealed and inserted into a temperature-controlled furnace at the reaction temperature of 160 °C for 16 h. The autoclave, once removed from the furnace, was allowed to cool down to room temperature naturally. The precipitate was collected by centrifugation, washed alternately with deionized water and ethanol, and dried in air under ambient conditions.

2.3 ***Characterization.*** Transmission electron microscopy (TEM) images were performed on a JEOL JEM-2010 (HT) transmission electron microscope at 200 kV, and the samples dissolved in water and dropped on carbon covered copper grids. High-resolution TEM (HRTEM) images and selected area electron diffraction (SAED) patterns were performed on a JEOL JEM-2100F transmission electron microscope at 200 kV, and the samples also dissolved in water and dropped on carbon covered copper grids. For measuring the composition of sample with Cu^{2+} precursor, the sample dropped on carbon covered gold grids. Field emission scanning electron microscopy (FSEM) studies were carried out using a FEI Sirion FEG and operated at 25 keV, samples were sprinkled onto the conductive substrate, respectively. Powder X-ray diffraction (XRD) patterns of the samples were recorded on a D/ruax2550PC (Japan) using Cu Kα radiation (λ = 0.1542 nm) operated at 40 kV and 40 mA and at a scan rate of 0.05° 2θ s^{-1}. The Raman scattering spectra of all the samples were collected using a micro-Raman system (LabRAM HR800). Lasers with wavelengths of 488 nm were used as the excitation sources.

2.4 ***Magnetic measurements.*** Magnetic measurements were performed on a Quantum Design physical property measurement system (PPMS) with equipped a vibrating sample magnetometer (VSM). The powder sample was filled in a diamagnetic plastic tube, and then the packed sample was put in a diamagnetic plastic straw and impacted into a minimal volume for magnetic measurements. Background magnetic measurements were checked for the packing

material. In the zero-field-cooled (ZFC) measurements, the samples were cooled from 300 to 10 K without applying an external field. After reaching 10 K, a field of 500 Oe was applied and the magnetic moments were recorded as the temperature increased. For field-cooled (FC) measurements, the samples were cooled from 300 K under an applied field of 500 Oe; then the magnetic moments were recorded as the temperature increased.

3. Results and Discussion

3.1 Outline view of cubic and thorhombic particles

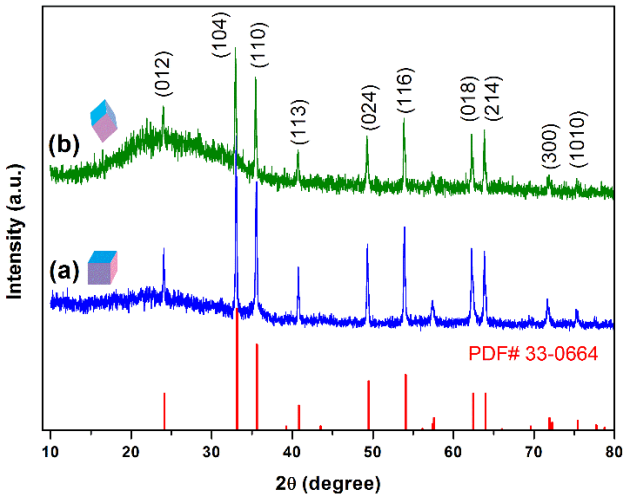

Fig. 1 XRD patterns of iron oxide NPs prepared with Zn2+ (curve a) and Cu2+ ions (curve b) as additive, respectively (drawn from the JCPDF files of hematite, are shown at the bottom).

Fig. 1 shows the XRD patterns of iron oxide NPs prepared with Zn^{2+} (curve a) and Cu^{2+} ions (curve b) as additive, respectively. All the diffraction peaks can be indexed to pure rhombohedral structure with a $R\bar{3}c$ space group for hematite (JCPDS 33-0664) and no characteristic peaks of impurities can be detected.[25] The results reveal that the Zn and Cu ions cannot form ZnO and CuO after reaction, respectively.

Fig. 2 shows the morphology of α-Fe_2O_3 particles prepared with Zn^{2+} and Cu^{2+} ions as additive, respectively. As shown in **Fig. 2a** and **Fig. 2b**, a representative large-area SEM image of the obtained α-Fe_2O_3 particles with the zinc ions as additive, illustrating that the majority of the sample is cubic shape containing 6 facets and 12 edges, and the edge length is about 300 nm. From the insert high-magnification SEM image in **Fig. 2b**, it can be seen that the surface of cubic α-Fe_2O_3 particles is not smooth, which consists of many irregular and randomly arranged protrusions. **Fig. 2c** and **Fig. 2d** shows the typical large-area SEM image of the obtained α-Fe_2O_3 particles with the cupric ions as additive, illustrating that the majority of the sample is quasi-thorhombic shape with an edge length of about 300 nm.

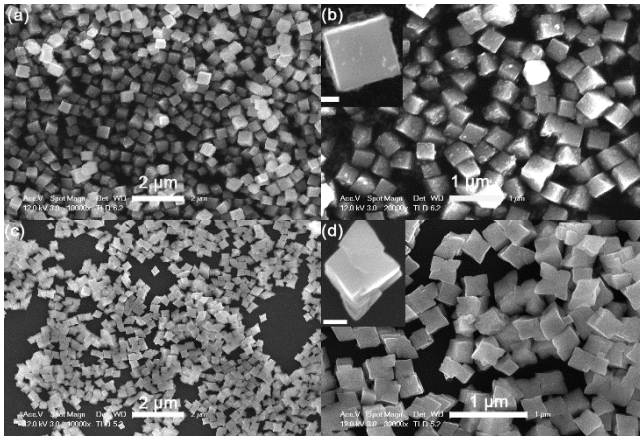

Fig. 2 SEM images of iron oxide NPs prepared with Zn^{2+} (a, b) and Cu^{2+} ions (c, d) as additive, respectively (the insert bar is 100 nm).

The overall scheme of the synthetic process is illustrated in **Scheme 1**. Without the addition of zinc or cupric precursor, only irregular α-Fe_2O_3 nanoparticles can be obtained (**Fig. S1**, in the *Support Information*). It is well known that metal ions can adsorb on the surface of α-Fe_2O_3, and the selective adsorption to α-Fe_2O_3 planes are different. The different adsorption properties to different metal ions of the different planes of α-Fe_2O_3 would lead to the formation of different α-Fe_2O_3 nanostructures with different exposed surfaces. We checked the $MnAc_2$, $CoAc_2$ and $NiAc_2$ as additive, respectively, when the mixture of ferric salt and ammonium solution was hydrothermally treated, only irregular iron oxide nanoparticles can be obtained (**Fig. S2**, in the *Support Information*). The above results reveal that the addition of Zn^{2+} or Cu^{2+} in the reaction system is the major reason for the formation of α-Fe_2O_3 particles with unique shape, and the edge length of particles is almost equal.

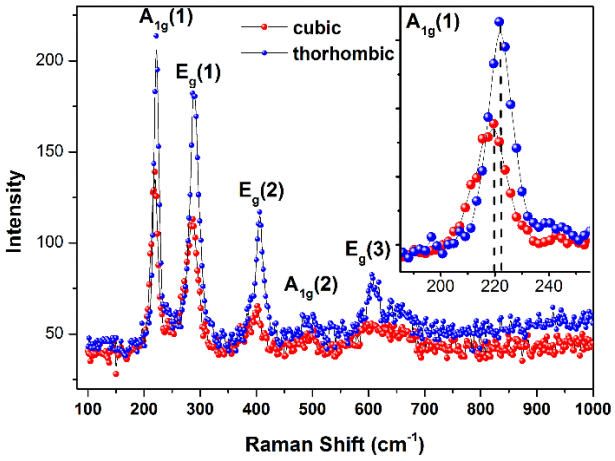

Fig. 3 Raman spectrum of α-Fe_2O_3 particles prepared with Zn^{2+} (cubic) and Cu^{2+} ions (thorhombic) as additive, respectively.

As shown in **Fig. 3**, the phase composition of α-Fe_2O_3 particles with different shapes were investigated by room-temperature Raman spectroscopy utilizing an excitation wavelength of 488 nm. Hematite belongs to the D_{3d}^6 crystal space group and the phonon lines are expected in the blue curve, which is a consensus on the reported data. And the five well-defined Raman peaks at about 220 and 497 cm^{-1}, 286, 406 and 612 cm^{-1} can be indexed to the A_{1g} and

E_g modes of α-Fe_2O_3, respectively. No unambiguous signal from other iron oxide phases or zinc/cupric ferrite phases was observed in the Raman spectra. The inset in **Fig. 3** shows a comparison of high-resolution Raman spectra of Fe A_{1g} (1) transitions of these two samples, the Raman shift of cubic α-Fe_2O_3 particles is 219.7 cm^{-1}, and the Raman shift of thorhombic α-Fe_2O_3 particles is 212.1 cm^{-1}, the red shift can be attributed to the phonon confinement effects and stress effects in the nanocrystals with different shapes.[26]

3.2 Cubic shape α-Fe_2O_3 particles

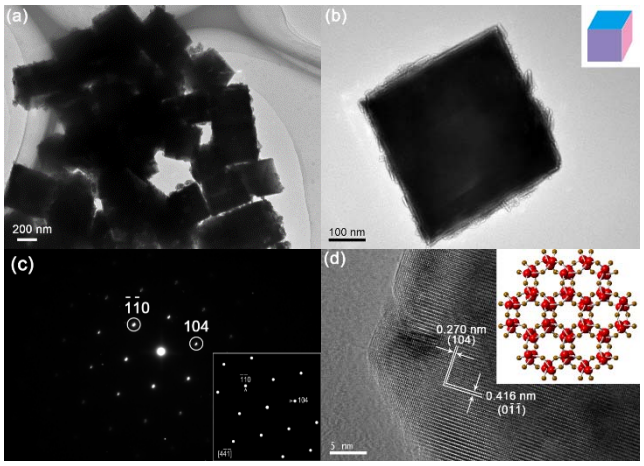

Fig. 4 TEM (a, b), typical SAED pattern (c, the insert is the calculated electronic diffraction pattern of $[44\bar{1}]$ projection) and HRTEM (d, insert is the crystal structure of α-Fe_2O_3) images of cubic iron oxide NPs prepared with Zn^{2+} ions as additive.

In order to understand the crystal structure of the cubic hematite particles, a systematic transmission electron microscopy investigation was carried out in detail. **Fig. 4a** shows the representative TEM image and **Fig. 4b** shows a single cubic α-Fe_2O_3 particles. These particles display a cubic profile, but with a highly roughened surface, which consists of many irregular and randomly arranged protrusions. **Fig. 4c** is the corresponding selected area electron diffraction (SAED) pattern of the single cubic α-Fe_2O_3 particles. The diffraction spots are attributed to $(\bar{1}\,\bar{1}0)$ and (104) planes and/or their equivalent planes under the incident electron beam along the $[44\bar{1}]$ direction. The sharp diffraction spots in **Fig. 4c** revealed that the single-crystalline nature of the cubic α-Fe_2O_3 particles. The SAED pattern was also calculated using theoretical simulation software with incident electron beam direction of $[44\bar{1}]$. The result of theoretical calculation, shown in the insert in the **Fig. 4c**, is consistent with the experiment result. **Fig. 4d** shows the HRTEM image were taken in the labelled region of **Fig. 4b**, two kinds of lattice fringes are identified, and their corresponding interplane distances are scaled to 0.270 and 0.416 nm, which can be assigned to the (104) and $(\bar{1}\,\bar{1}0)$ planes of α-Fe_2O_3, respectively. On the basis of the above analysis, it was concluded that the longitudinal direction of the cubic hematite is $[44\bar{1}]$. And the SAED patterns are consistent with the interplane distances results.

3.3 Thorhombic shape α-Fe_2O_3 particles

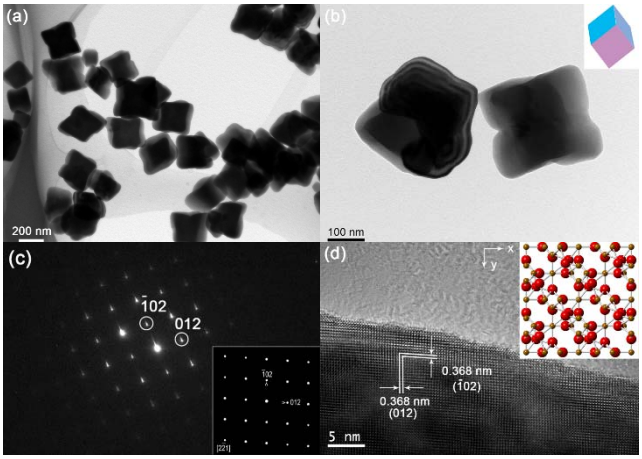

Fig. 5 TEM (a, b), typical SAED pattern (c, the insert is the calculated electronic diffraction pattern of $[2\bar{2}1]$ projection) and HRTEM (d, insert is the crystal structure of α-Fe_2O_3) images of thorhombic iron oxide NPs prepared with Cu^{2+} ions as additive.

Comparing the structures of cubic hematite particles, **Fig. 5a** shows the representative TEM image of thorhombic hematite particles. **Fig. 5b** shows the magnified TEM image of two particles, it can be seen that the edges are not straight, some blending can be found. **Fig. 5c** is the corresponding SAED pattern of the single thorhombic α-Fe_2O_3 particles. The diffraction spots are attributed to $(\bar{1}02)$ and (012) planes and/or their equivalent planes under the incident electron beam along the $[2\bar{2}1]$ direction. The diffraction spots in **Fig. 5c** revealed that the single-crystalline nature of the cubic α-Fe_2O_3 particles. The SAED pattern was also calculated using theoretical simulation software with incident electron beam direction of $[2\bar{2}1]$. The result of theoretical calculation, shown in the insert in the **Fig. 5c**, is consistent with the current experiment result. **Fig. 5d** shows the HRTEM image were taken in the labelled region of **Fig. 5b**, two kinds of lattice fringes are identified, and their corresponding interplane distances both are scaled to 0.368 nm, which can be assigned to the (012) and $(\bar{1}02)$ planes of α-Fe_2O_3, respectively. Similar results could be obtained from the SAED pattern.

As shown in **Fig. 6**, energy-dispersive X-ray (EDX) analysis was used to determine the elemental composition of the nanoparticles, mainly to confirm the presence of the dopant atoms within the α-Fe_2O_3 nanoparticles and to calculate the effective dopant concentration. Both the EDX spectra of the cubic and thorhombic α-Fe_2O_3 particles revealed that the presence of Fe and O elements. And the introduction of Zn and Cu element can be verified by EDX analysis. The introduced concentration of Zn and Cu is 2.3 wt% and 6.7 wt%, respectively. The results illustrate the metal ions have been introduced in the formation process of α-Fe_2O_3 particles. Moreover, the Zn and Cu elements can be observed in the total morphology evolution stage, and the results were depicted in **Fig. S3** (*Support Information*).

It is worth noting that the only difference between the preparation conditions of cubic and thorhombic particles was the types of metal ions. This implied that the metal ions may play an important role in tuning the particle shape. Therefore, the morphology evolution of the cubic and thorhombic α-Fe_2O_3 particles with different reaction time have been investigated, and the results have been present in **Fig. S4** and **Fig. S5** (*Support Information*). The growth of α-Fe_2O_3 on the initial crystal nuclei

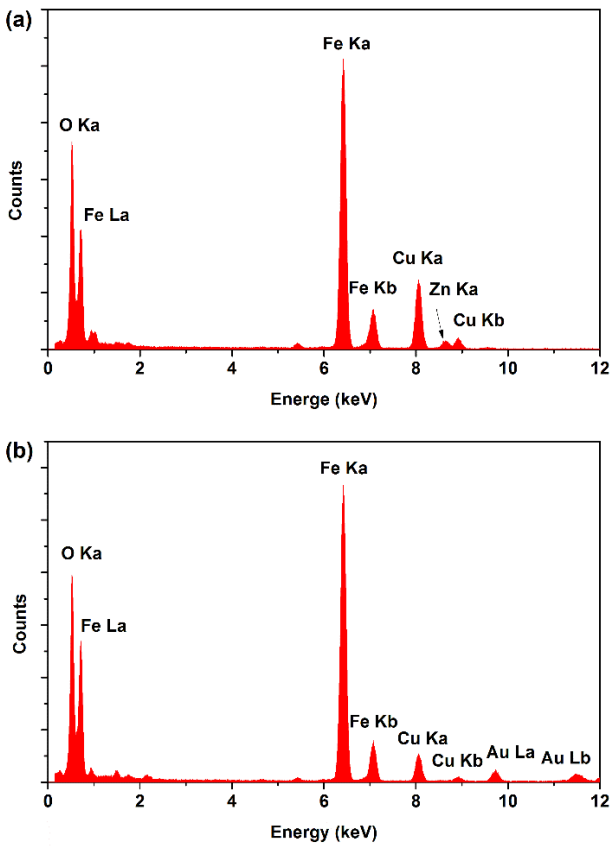

Fig. 6 EDX spectra of single cubic α-Fe_2O_3 particles (a, Cu element comes from the copper grid) and thorhombic α-Fe_2O_3 particles (b, Au element comes from the gold grid).

occurred on the sites on which Fe^{3+} cations could be adsorbed. Thus, fast growth would occur on those planes that adsorbed more Fe^{3+} cations. In aqueous solution, the sustaining adsorption of Fe^{3+} cations on Fe_2O_3 crystal nuclei is mainly through their coordination with the surface hydroxyl.[27] When Cu ions and Zn ions were introduced into the reaction, the coordinate reaction with surface hydroxyl can be occurred simultaneously. Therefore, when the α-Fe_2O_3 nuclei were formed in the solution, the adsorption of Zn or Cu ions on α-Fe_2O_3 would inevitably occur. As a result, the adsorption of Zn ions and Cu ions may play an important role in the growth of cubic and thorhombic particles, respectively. The different adsorption properties to different metal ions of the different planes of α-Fe_2O_3 would lead to the formation of different α-Fe_2O_3 nanostructures with different exposed surfaces. As shown in **Fig. S4**, it can be seen that α-Fe_2O_3 undergoes an evolution from small nanoparticles to cubic particles. As shown in **Fig. S4a**, many small nanoparticles can be observed in the as-obtained samples, and when the reaction time extending to 8 h, the proportion of small nanoparticles is clearly decreased. The results reveal that a typical Ostwald ripening process involving the formation of larger crystals by greatly reducing the interfacial energy of small primary nanocrystals is energetically favoured. The addition of zinc or copper precursor in the reaction system is no doubt the reason for the formation of α-Fe_2O_3 bound by the high-index facets. Carefully comparing the evolution process of the two particles by HRTEM, we found that the exposed plane of (012) is hardly to find in the cubic α-Fe_2O_3 particles (**Fig. S4d-S4f** and **Fig. 5d**), which can be

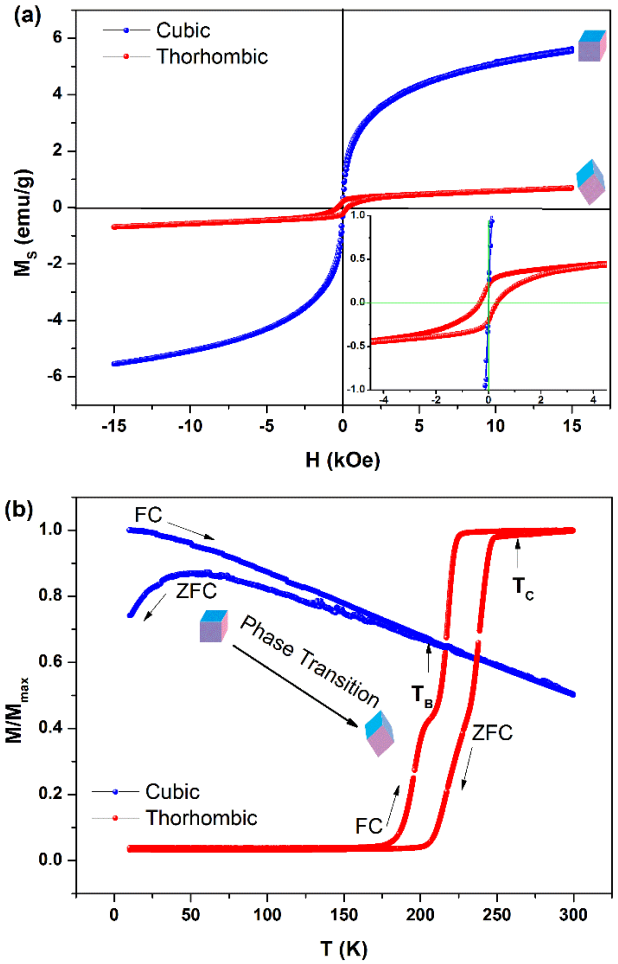

Fig. 7 Magnetic hysteresis loops of cubic and thorhombic α-Fe_2O_3 particles (a, T = 300 K), temperature dependence of ZFC and FC magnetic moments of cubic and thorhombic α-Fe_2O_3 particles at applied fields of 500 Oe.

easily found in thorhombic α-Fe_2O_3 particles (**Fig. S5d-S5f** and **Fig. 4d**), and the exposed plane of (104) can be easily found in the cubic α-Fe_2O_3 particles. Thus, an important conclusion can be drawn: The Cu ions are beneficial to the growth of (012) exposed planes, and the Zn ions are beneficial to the growth of (104) exposed planes. Therefore, the Zn ions and Cu ions can bound the different facets and thus the cubic and thorhombic α-Fe_2O_3 particles can be synthesized separately in high yields.

3.4 Shape dependent magnetic properties

The cubic and thorhombic α-Fe_2O_3 particles were investigated in terms of hysteresis loops (M-H curves) and field cooling (FC) and zero field cooling (ZFC) magnetization curves. The room-temperature magnetic hysteresis measurements of the samples were carried out at 300 K in the applied magnetic field sweeping from -15 to 15 kOe. As shown in **Fig. 7a**, the saturation magnetization (M_S) of the cubic and thorhombic α-Fe_2O_3 particles were found to be 5.63 and 0.6 emu g^{-1} at 300 K, respectively. Additionally, the thorhombic α-Fe_2O_3 particles display a remanent magnetization (M_r) of 0.22 emu g^{-1} and coercivity (H_C) of 314 Oe (see the insert magnified image of **Fig. 7a**), suggesting that the thorhombic α-Fe_2O_3 particles exhibit ferromagnetic behaviours.

However, the as-prepared cubic α-Fe_2O_3 particles exhibit no remanent magnetization and coercivity. For the cubic α-Fe_2O_3 particles, the FC/ZFC curves obtained at different temperatures were shown in **Fig. 7b** clearly shows the presence of blocking temperature (T_B) around 200 K. On the other hand, the lack of hysteresis at room temperature is evident from the insert of **Fig. 7a**. The observation of superparamagnetic blocking and the absence of magnetic remanence directly demonstrate that the samples are superparamagnetic at room temperature. However, the thorhombic α-Fe_2O_3 particles present a clear low-temperature phase reverse transition behaviours, which exhibit as antiferromagnetic properties at T < 175 K, and transfer to ferromagnetic properties when the temperature above 175 K. And the Curie temperatures (T_C) can just be observed, the value is about 270 K.

4 Conclusions

In conclusion, uniform hematite nanoparticles with cubic and thorhombic shapes via zinc and copper ions mediate hydrothermal route have been synthesized, respectively. The experimental investigations provided insight on the role of the metal (atomic number from 25 to 30) ions used in the synthetic process and a diagram schematically illustrating formation of this morphology was also proposed. The experimental results show that the metal ion play important roles in the formation of iron oxide nanomaterials with different morphologies. The developed method represents a highly economical and facile ‘‘green’’ process for the tunable synthesis of hematite particles. Moreover, the magnetic property of our products were evaluated, and the results show that these α-Fe_2O_3 nanoparticles exhibit an interesting shape-dependent magnetic properties, which would be a class of promising functional material for many applications. However, extensive experiments should be performed on this α-Fe_2O_3 structure to understand better its other properties for practical applications.

Acknowledgment

The author thanks the NSFC (51201115, 51171132), China Postdoctoral Science Foundation (2012M511661), Hong Kong Scholars Program, the Fundamental Research Funds for the Central Universities, Young Chenguang Project of Wuhan City (2013070104010011).

Notes and references

[a] *Laboratory of Functional Nanomaterials and Printed Electronics, School of Printing and Packaging, Wuhan University, Wuhan 430072, P. R. China. Fax: +86-27-68778433; Tel: +86-27-68778529; E-mail: weiwu@whu.edu.cn*

[b] *Key Laboratory of Artificial Micro- and Nano-structures of Ministry of Education, Center for Electronic Microscopy and School of Physics and Technology, Wuhan University, Wuhan 430072, P. R. China. E-mail: czjiang@whu.edu.cn*

[c] *State Key Laboratory for Powder Metallurgy, Central South University, Changsha 410083, P. R. China*

 # the authors contributed equally to this work.

† Electronic Supplementary Information (ESI) available: [The TEM image of the samples without any ion additive and with Ni^{2+}, Mn^{2+}, Co^{2+} ions additive present in reaction process, the TEM, HRTEM and EDX of the morphology evolution of the cubic α-Fe_2O_3 particles with different reaction time from 1h to 8 h.]. See DOI: 10.1039/b000000x/

1. W. Wu, Q. G. He and C. Z. Jiang, *Nanoscale Res. Lett.* , 2008, **3**, 397-415.
2. D. Ling and T. Hyeon, *Small*, 2013, **9**, 1450-1466.
3. G. Tong, J. Guan and Q. Zhang, *Adv. Funct. Mater.* , 2013, **23**, 2406-2414.
4. J. Guan, L. Liu, L. Xu, Z. Sun and Y. Zhang, *Crystengcomm*, 2011, **13**, 2636-2643.
5. G. Tong, J. Guan, Z. Xiao, F. Mou, W. Wang and G. Yan, *Chem. Mater.* , 2008, **20**, 3535-3539.
6. J. Watt, S. Cheong and R. D. Tilley, *Nano Today*, 2013, **8**, 198-215.
7. W. Wu, X. H. Xiao, F. Ren, S. F. Zhang and C. Z. Jiang, *J. Low Temp. Phys.* , 2012, **168**, 306-313.
8. W. Wu, X. H. Xiao, S. F. Zhang, T. C. Peng, J. Zhou, F. Ren and C. Z. Jiang, *Nanoscale Res. Lett.* , 2010, **5**, 1474-1479.
9. X. Mou, X. Wei, Y. Li and W. Shen, *Crystengcomm*, 2012, **14**, 5107-5120.
10. F. Mou, J. Guan, H. Ma, L. Xu and W. Shi, *ACS Appl. Mater. Interfaces* 2012, **4**, 3987-3993.
11. J. Guan, G. Yan, W. Wang and J. Liu, *J. Mater. Chem.* , 2012, **22**, 3909-3915.
12. F. Mou, J. Guan, Z. Xiao, Z. Sun, W. Shi and X.-a. Fan, *J. Mater. Chem.* , 2011, **21**, 5414-5421.
13. X. a. Fan, J. Guan, Z. Li, F. Mou, G. Tong and W. Wang, *J. Mater. Chem.* , 2010, **20**, 1676-1682.
14. B. Bateer, C. Tian, Y. Qu, S. Du, T. Tan, R. Wang, G. Tian and H. Fu, *Crystengcomm*, 2013, **15**, 3366-3371.
15. R. Xu, H. Yan, W. He, Y. Su, J.-C. Nie and L. He, *J. Phys. Chem. C*, 2012, **116**, 6879-6883.
16. C. J. Jia, L. D. Sun, F. Luo, X. D. Han, L. J. Heyderman, Z. G. Yan, C. H. Yan, K. Zheng, Z. Zhang, M. Takano, N. Hayashi, M. Eltschka, M. Klaui, U. Rudiger, T. Kasama, L. Cervera-Gontard, R. E. Dunin-Borkowski, G. Tzvetkov and J. Raabe, *J. Am. Chem. Soc.* , 2008, **130**, 16968-16977.
17. X. Huang, J. Guan, Z. Xiao, G. Tong, F. Mou and X. a. Fan, *J. Colloid Interface Sci.* , 2011, **357**, 36-45.
18. J. B. Rivest and P. K. Jain, *Chem. Soc. Rev.* , 2013, **42**, 89-96.
19. Y. Yang, H. Ma, J. Zhuang and X. Wang, *Inorg. Chem.* , 2011, **50**, 10143-10151.
20. T.-K. Van, H. G. Cha, C. K. Nguyen, S.-W. Kim, M.-H. Jung and Y. S. Kang, *Cryst. Growth Des.*, 2012, **12**, 862-868.
21. Z.-F. Dou, C.-Y. Cao, Q. Wang, J. Qu, Y. Yu and W.-G. Song, *ACS Appl. Mater. Interfaces* 2012, **4**, 5698-5703.
22. J. Ma, X. Zhang, K. Chen, G. Li and X. Han, *J. Mater. Chem. A*, 2013, **1**, 5545-5553.
23. B. Lv, Z. Liu, H. Tian, Y. Xu, D. Wu and Y. Sun, *Adv. Funct. Mater.* , 2010, **20**, 3987-3996.
24. J. Choi, J. Cha and J.-K. Lee, *RSC Advances*, 2013, DOI: 10.1039/C1033RA40283E.
25. W. Wu, X. H. Xiao, S. F. Zhang, J. A. Zhou, L. X. Fan, F. Ren and C. Z. Jiang, *J. Phys. Chem. C* 2010, **114**, 16092-16103.
26. C. Baratto, P. P. Lottici, D. Bersani, G. Antonioli, G. Gnappi and A. Montenero, *J. Sol-Gel Sci. Technol.* , 1998, **13**, 667-671.
27. V. Barrón and J. Torrent, *J. Colloid Interface Sci.* , 1996, **177**, 407-410.

Graphic Abstract

Metal Ion-Mediated Synthesis and Shape-dependent Magnetic Properties of Single-Crystalline α-Fe_2O_3 Nanoparticles

W. Wu, S. L. Yang, J. Pan, L. L. Sun, J. Zhou, Z. G. Dai, X. H. Xiao, H. B. Zhang and C. Z. Jiang

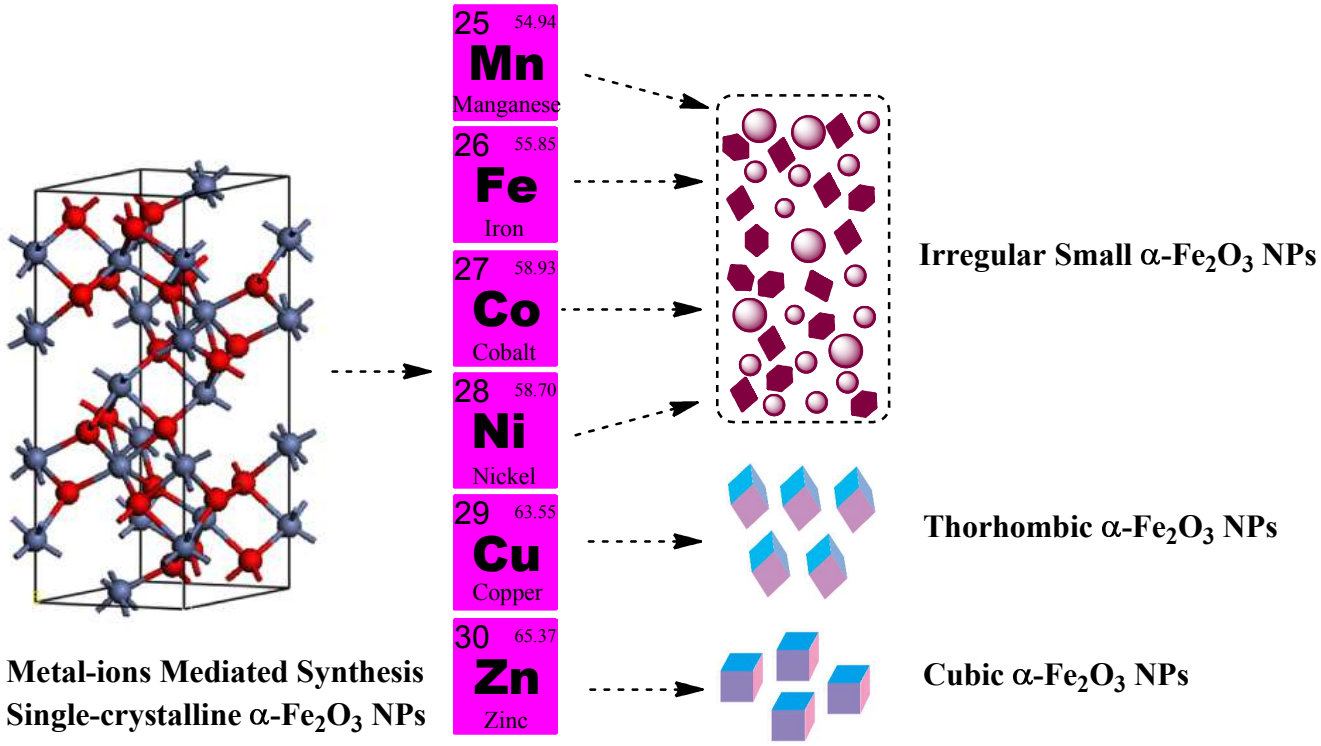

Some useful insights into the synthesis and shape-dependent magnetic properties of iron oxide nanoparticles with different morphologies have been present.